The Astrophysical Journal, 690:1585–1589, 2009 January 10 doi:10.1088/0004-637X/690/2/1585

ANOMALOUS MICROWAVE EMISSION FROM THE H II REGION RCW175

C. Dickinson[1], R. D. Davies[2], J. R. Allison[3], J. R. Bond[4], S. Casassus[5], K. Cleary[6], R. J. Davis[2], M. E. Jones[3], B. S. Mason[7], S. T. Myers[8], T. J. Pearson[6], A. C. S. Readhead[6], J. L. Sievers[4], A. C. Taylor[3], M. Todorović[2], G. J. White[9], and P. N. Wilkinson[2]

[1] Infrared Processing and Analysis Center, California Institute of Technology, M/S 220-6, 1200 E. California Blvd., Pasadena, CA 91125, USA
[2] Jodrell Bank Observatory, University of Manchester, Lower Withington, Macclesfield, Cheshire, SK11 9DL, UK
[3] Oxford Astrophysics, University of Oxford, Denys Wilkinson Building, Keble Road, Oxford, OX1 3RH, UK
[4] Canadian Institute for Theoretical Astrophysics, University of Toronto, Toronto, Canada
[5] Departamento de Astronomía, Universidad de Chile, Casilla 36-D, Santiago, Chile
[6] Chajnantor Observatory, California Institute of Technology, M/S 105-24, Pasadena, CA 91125, USA
[7] National Radio Astronomy Observatory, Green Bank, WV, USA
[8] National Radio Astronomy Observatory, Socorro, NM, USA
[9] Rutherford Appleton Laboratory, Didcot, OX11 0QX, UK

Received 2008 July 24; accepted 2008 September 11; published 2008 December 22

ABSTRACT

We present evidence for anomalous microwave emission in the RCW175 H II region. Motivated by 33 GHz 13′ resolution data from the Very Small Array (VSA), we observed RCW175 at 31 GHz with the Cosmic Background Imager (CBI) at a resolution of 4′. The region consists of two distinct components, G29.0-0.6 and G29.1-0.7, which are detected at high signal-to-noise ratio. The integrated flux density is 5.97 ± 0.30 Jy at 31 GHz, in good agreement with the VSA. The 31 GHz flux density is 3.28 ± 0.38 Jy (8.6σ) above the expected value from optically thin free–free emission based on lower frequency radio data and thermal dust constrained by *IRAS* and *WMAP* data. Conventional emission mechanisms such as optically thick emission from ultracompact H II regions cannot easily account for this excess. We interpret the excess as evidence for electric dipole emission from small spinning dust grains, which does provide an adequate fit to the data.

Key words: ISM: individual (RCW175) – radiation mechanisms: general – radio continuum: ISM

1. INTRODUCTION

In recent years there has been mounting observational evidence for a new diffuse component emitting at frequencies ≈10–60 GHz. The anomalous microwave emission was first detected at 14 and 32 GHz by Leitch et al. (1997). Since then, a similar picture has emerged both at high latitudes (Banday et al. 2003; de Oliveira-Costa et al. 2004; Fernández-Cerezo et al. 2006; Hildebrandt et al. 2007; Bonaldi et al. 2007) and from individual Galactic sources (Casassus et al. 2004, 2006, 2007; Watson et al. 2005; Scaife et al. 2007; Dickinson et al. 2007), although negative detections have also been reported (Dickinson et al. 2006; Scaife et al. 2008). The spectral index between 20 and 40 GHz is $\alpha \approx -1.1$ (Davies et al. 2006) with some evidence of flattening at $\sim$ 10–15 GHz (Leitch et al. 1997; de Oliveira-Costa et al. 2004; Hildebrandt et al. 2007). The emission appears to be very closely correlated with far-IR data suggesting a dust origin. Various emission mechanisms have been suggested, including hot ($T \sim 10^6$ K) free–free (Leitch et al. 1997), flat spectrum synchrotron (Bennett et al. 2003), spinning dust (Draine & Lazarian 1998a, 1998b), and magnetic dust (Draine & Lazarian 1999). The overall picture is still very unclear and new data covering the range 10–60 GHz are urgently needed.

RCW175 (Rodgers et al. 1960) is a diffuse H II region, which consists of a "medium brightness" optical filament (G29.1-0.7, S65) $\sim 7' \times 5'$ in extent, and a nearby compact source (G29.0-0.6), which is heavily obscured by dust. Although the filament is clearly seen in high-resolution data, the compact counterpart is considerably brighter. The ionization is thought to be provided by a single B-1 II type star, which forms part of a five-star cluster (Forbes 1989; Sharpless 1959) at a distance of 3.6 kpc.

Observations made with the Very Small Array (VSA) at 33 GHz (Watson et al. 2003; Dickinson et al. 2004) as part of a Galactic plane survey (M. Todorović et al. 2009, in preparation) indicate that RCW175 is anomalously bright by a factor of ≈ 2, when compared with lower frequency data. In this paper, we present accurate Cosmic Background Imager (CBI) 31 GHz observations of RCW175 and make a comparison with ancillary radio/far-infrared (FIR) data. We find that the emission at 31 GHz is significantly above what is expected from a simple model of free–free and vibrational dust emissions.

2. DATA

2.1. 31 GHz: Cosmic Background Imager

The CBI is a 26–36 GHz 13-element comounted interferometer, operated at the Chajnantor Observatory, Chile. The original CBI used 0.9 m dishes to provide high temperature sensitivity measurements on angular scales $\sim$ 30′–6′(Padin et al. 2002; Readhead et al. 2004). Recently, it has been upgraded with 1.4 m dishes (CBI2) to give increased temperature sensitivity on angular scales $\approx$ 4′–15′(A. C. Taylor et al. 2009, in preparation).

We observed RCW175 at R.A. $= 18^{\rm h}46^{\rm m}40^{\rm s}$, decl. $= -03^{\rm d}46^{\rm m}00^{\rm s}$ (J2000), on four nights in May 2007, with a total integration time of 6 hr with CBI2. Boresight rotations of the array were used to improve the u, v-coverage. Ground spillover was removed by subtracting observations of a comparison field, 8 minutes later in right ascension, observed at the same hour angles. Jupiter was the primary amplitude/phase calibrator with absolute calibration tied to a Jupiter temperature of 146.6 ± 0.75 K at 33 GHz (Hill et al. 2008). Observations of secondary calibrators showed that the pointing was good to better than 1′.

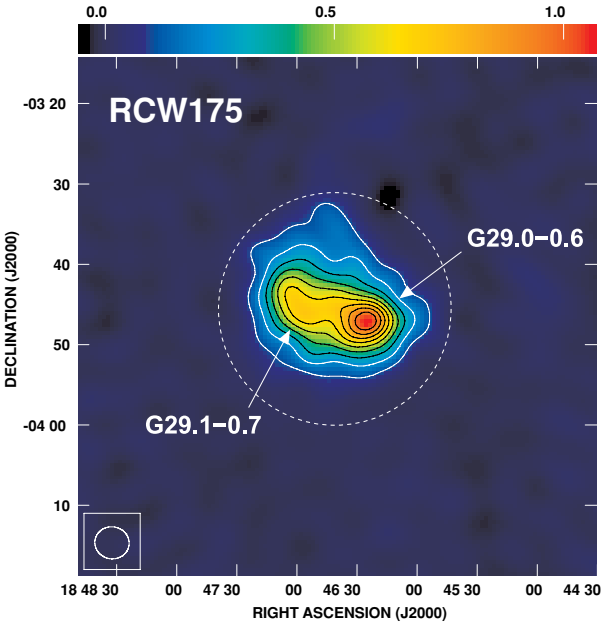

Figure 1. CBI 31 GHz CLEANed map of the RCW175 region. Contours are at 10, 20, 30, 40, 50, 60, 70, 80, 90% of the peak brightness, 1.04 Jy beam^{-1}. The CBI primary beam (FWHM) is shown as a dashed line.

A uniform-weighted, CLEANed map is shown in Figure 1. The synthesized beam is $4\farcm3 \times 4\farcm0$ and the primary beam is approximately Gaussian with FWHM $28\farcm2$ (30 GHz/ν). Corrections for the primary beam were made directly to the CLEAN components at each frequency; the bulk of the emission fits well within the extent of the primary beam. The total flux density in the map is 6.4 Jy with a peak brightness of 1.04 Jy beam^{-1} and the noise level is 27 mJy beam^{-1}.

The CBI map detects and resolves both components in the RCW175 region. G29.0-0.6 in the west is more compact and is significantly brighter than the more diffuse G29.1-0.7 in the east. Although there is some extended emission almost all (93%) of the flux can be fitted by two Gaussian components. Note that the entire extent of RCW175 is equivalent to ≈ 13 beam areas; thus the maximum CLEAN bias is ≈ 0.35 Jy. We fitted two elliptical Gaussians plus a baseline offset using the aips task jmfit. At 31 GHz we find that G29.0-0.6 has a deconvolved size $5\farcm4 \times 5\farcm1$ and integrated flux density, $S_i = 2.20$Jy. G29.1-0.7 is $10\farcm0 \times 8\farcm2$ and $S_i = 3.76$ Jy. Simulations showed that CBI flux loss due to the limited u, v-coverage is $\lesssim 10\%$ when fitting two Gaussians to the bulk of the emission.

2.2. Ancillary Radio/FIR Data

Table 1 lists frequencies, angular resolutions, and references for the data[10] used in this paper, and Figure 2 shows selected maps centered on RCW175. The radio maps from 1.4 GHz to 14.35 GHz show enhanced emission at the same location as that seen in the CBI image with the bright, more compact, hotspot in the west (G29.0-0.6) and the fainter component to the east (G29.1-0.7). For data with resolutions $\sim 4'$, the subcomponents are not well separated and the bulk of the emission is confined to a region $\sim 10' \times 5'$. At these resolutions the region looks like one extended object with G29.0-0.6 dominating at one end. The higher resolution NVSS 1.4 GHz/*Spitzer* 24 μm data show the more compact G29.0-0.6 has an extent of $\approx 2'$. A filament of emission to the east (G29.1-0.7) is coincident with the filament seen in high-resolution optical/IR images. There is low-level emission in the region in between, which is particularly evident in the 24 μm image.

WMAP 5 yr total-intensity maps (Hinshaw et al. 2008) covering 23–94 GHz show no significant detection of emission above the Galactic background at the location of RCW175. The 94 GHz map, at $\approx 12\farcm6$ resolution, is, however, useful for placing an upper limit on the thermal dust contribution (see Section 3.1).

3. FLUX DENSITY SPECTRUM

3.1. Integrated Flux Density Spectrum

The integrated flux density in each map was calculated both by fitting multiple Gaussians (with baseline offset) and by integrating over a given aperture. For the interferometric data, both methods gave roughly consistent results within the errors. For total-power data, the aperture value could be overestimated due to the background level. Moreover, a possible offset of $\sim 0\farcm5$ in the CBI map could result in a bias depending on the exact aperture location; an offset of $\approx 0\farcm5$ does appear to be visible when comparing CBI contours with the NVSS 1.4 GHz map (Figure 2). For these reasons, we chose the Gaussian fitting method as described in Section 2.1.

Integrated flux densities for RCW175 and the G29.0-0.6 component are given in Table 1 and plotted in Figure 3. Absolute calibration errors (assumed to be 10% if not known) were added in quadrature to the fitting error reported by jmfit. We include the 33 GHz value for RCW175 from the VSA, which is in good agreement with the CBI value. The lower resolution ($\approx 13'$) VSA data meant that a single Gaussian fit was adequate and that flux loss was negligible. Since there is a correction factor of 1.53 for the primary beam at the position of RCW175, we assigned a conservative 10% error to account for any small deviations from the assumed Gaussian primary beam. An upper limit was inferred from the *WMAP W*-band (94 GHz) map by fitting for a parabolic baseline in the vicinity of RCW175 to account for the Galactic background, and calculating the 3σ of the residual map.

3.2. SED Fitting

For a classical H II region, the radio/microwave spectrum consists of free–free emission at radio wavelengths and vibrational dust emission at infrared wavelengths. At the lowest radio frequencies (typically $\lesssim 1$ GHz), the free–free emission is optically thick and follows a $\alpha \approx +2$ spectrum.[11] Above the turnover frequency (typically ~ 1 GHz), the emission becomes optically thin and follows a $\alpha \approx -0.1$ power law, with very little dependence on physical conditions (Rybicki & Lightman 1979; Dickinson et al. 2003). At high frequencies (typically > 100 GHz), vibrational dust emission becomes dominant. Vibrational dust is well represented by a modified blackbody function, $\nu^{\beta+2}B(\nu, T_{\rm dust})$, where β is the dust emissivity index and $B(\nu, T_{\rm dust})$ is the blackbody function for a given dust temperature, $T_{\rm dust}$.

The spectral energy distribution (SED) for RCW175 and the G29.0-0.6 component is shown in Figure 3. The low-frequency (<15 GHz) data were fitted by an optically thin

[10] Data were downloaded from the *Skyview* Web site (http://skyview.gsfc.nasa.gov), the MPIfR Image Survey Sampler Web site (http://www.mpifr-bonn.mpg.de/survey.html), the LAMBDA Web site (http://lambda.gsfc.nasa.gov/), and the IRSA Web site (http://irsa.ipac.caltech.edu).

[11] Throughout this paper, we use the spectral index convention for flux density given by $S \propto \nu^{\alpha}$.

Table 1
Flux Densities for RCW175 and G29.0-0.6

Frequency (GHz)	Telescope/ Survey	Angular Resolution (arcmin)	Reference For Data	Flux Density RCW175 (Jy)	Flux Density G29.0-0.6 (Jy)
1.4	Green Bank 300 ft	9.4 × 10.4	Altenhoff et al. (1970)	6.0 ± 1.8	Not resolved
2.7	Effelsberg 100 m	4.3	Reich et al. (1990)	3.83 ± 0.38	1.70 ± 0.17
5	Parkes 64 m	4.1	Haynes et al. (1978)	3.90 ± 0.39	1.30 ± 0.71
8.35	Green Bank 13.7 m	9.7	Langston et al. (2000)	2.68 ± 0.35	Not resolved
10	Nobeyama 45 m	3	Handa et al. (1987)	Not reported	1.39 ± 0.14
14.35	Green Bank 13.7 m	6.6	Langston et al. (2000)	3.21 ± 1.83	Not resolved
31	CBI	4.3 × 4.0	This work	5.97 ± 0.30	2.20 ± 0.33
33	VSA	13.1 × 10.0	M. Todorović et al. (2009, in preparation)	6.83 ± 0.68	Not resolved
94	*WMAP*	≈ 12.6	Hinshaw et al. (2008)	$< 4.5(3\sigma)$	$< 4.5(3\sigma)$
2997 (100 μm)	*IRAS*	≈ 4	Beichman et al. (1988)	18320 ± 10190	6970 ± 2930
4995 (60 μm)	*IRAS*	≈ 4	Beichman et al. (1988)	5864 ± 1292	4131 ± 548
12875 (24 μm)	*Spitzer* MIPSGAL	0.033	http://irsa.ipac.caltech.edu/	Not fitted	Not fitted

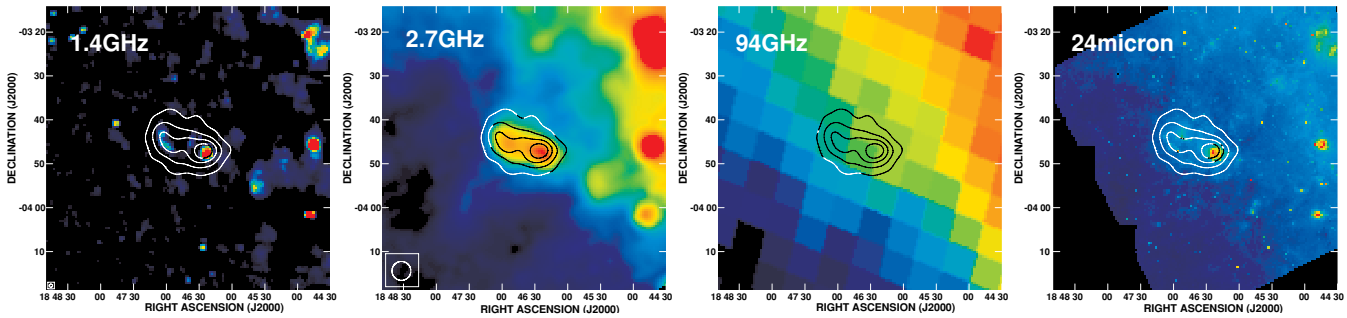

Figure 2. Multifrequency maps of the RCW175 region. From left to right: NVSS 1.4 GHz, Effelsberg 2.7 GHz, *WMAP* 94 GHz, and *Spitzer* MIPS 24 μm. Angular resolutions and references are given in Table 1. Contours are CBI 31 GHz at 20%, 40%, 60%, 80% of the peak brightness, 1.04 Jy beam^{-1}.

free–free power-law spectrum ($S \propto \nu^{\alpha}$) fixed to the theoretical value, $\alpha = -0.12$ for $T_e \approx 8000$ K and frequencies around ∼10 GHz. When fitting for the index we found $\alpha = -0.32 \pm 0.15$, which is consistent with this value. The infrared data (60/100 μm) were fitted by a single temperature dust component using a simple modified blackbody curve, $S \propto \nu^{\beta+2} B(\nu, T_{\rm dust})$. We did not attempt to fit data at shorter wavelengths. Since there are no data points in the submillimeter (∼ 100–1000 GHz), the emissivity index was fixed at $\beta = +2.0$, which is typical for H II regions (e.g., Gordon 1988). Flatter indices in the range $\beta \approx 1$–2 have been observed while the preferred value for $T_{\rm dust} \approx 30$ K is $\beta \approx +1.6$ (Dupac et al. 2003). However, the 94 GHz upper limit does not allow flatter indices than $\beta \approx 2$. The best-fitting dust temperatures were $T_{\rm dust} = 30.1 \pm 5.7$ K and $T_{\rm dust} = 37.6 \pm 6.4$ K, for RCW175 and G29.0-0.6, respectively.

From Figure 3 it is clear that the ∼ 30 GHz flux densities are significantly higher than the simple model can allow for. This model predicts a 31 GHz flux density for RCW175 of 2.69 ± 0.24 Jy, compared to the measured value of 5.97 ± 0.30 Jy. This corresponds to an excess over the free–free emission of 3.28 ± 0.38 Jy (8.6σ). Adopting the best-fit spectral index at low frequencies results in a larger excess at 31 GHz, although at a reduced significance level (6.4σ) due to the increased error when fitting for an additional parameter. The brighter component of G29.0-0.6 shows a similar level of excess (Figure 3).

4. DISCUSSION

A peaked (convex) spectrum is required to produce excess emission at ∼ 30 GHz without exceeding the upper limit at 94 GHz. The 3σ upper limit at 94 GHz strongly rules out a cold thermal dust component, or a flatter dust emissivity. Convex spectra can be produced by optically thick ultracompact (UC) H II regions, gigahertz-peaked spectrum (GPS) sources, or some new mechanism such as electrodipole and magnetodipole radiation.

UC H II regions are self-absorbed up to higher frequencies because of extremely high densities. Indeed it is possible to fit the radio data including the VSA/CBI data by including a homogenous compact H II region with angular size ∼ 1″ and emission measure of ∼ 3×10^9 cm^{-6} pc. Such parameters are within observed limits (Wood & Churchwell 1989). However, the additional component produces too much flux (≳10 Jy) at 94 GHz. For the same reasons, magnetodipole radiation can also be excluded as a major contributor.

GPS sources are high redshift radio sources in which the radio jets have been highly confined and the synchrotron emission is self-absorbed. A search through the NVSS catalog (Condon et al. 1998) revealed no bright (≳ 100 mJy) compact radio sources in this region and no bright (≳ 20 mJy), point-like sources appear in the NVSS 1.4 GHz map.

The anomalous emission could be due to electric dipole radiation from small rapidly spinning dust grains. If such grains have a residual dipole moment and spin at GHz frequencies, they will emit over a narrow range of frequencies. Figure 3 shows a typical spinning dust spectrum using the model of Draine & Lazarian (1998b) for the Cold Neutral Medium (CNM), scaled to fit the VSA/CBI data. The highly peaked spectrum allows an adequate fit to the data both at ∼ 10 GHz and yet consistent with the 94 GHz upper limit. We note that the appropriate model for Warm Ionized Medium (WIM) peaks at a slightly lower frequency and predicts too much flux at ∼ 10 GHz. Similarly, the Molecular Cloud (MC) model peaks at too high a frequency resulting in too much flux at 94 GHz. The peak intensity must therefore lie close to 30 GHz. However, the models are fairly

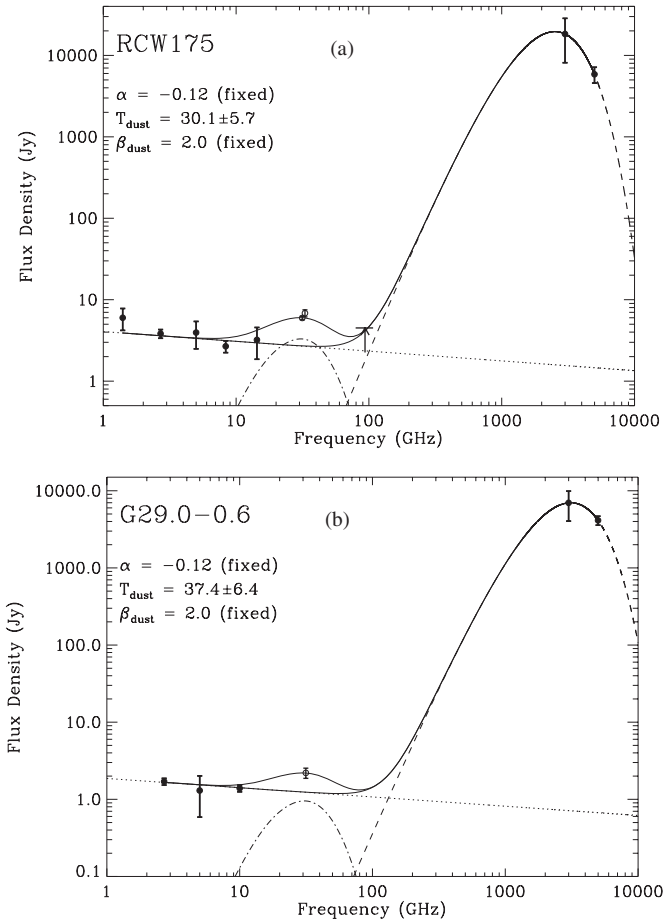

Figure 3. Integrated flux density spectrum for (a) both components combined (RCW175) and (b) the brighter component (G29.0-0.6). The filled circles represent data fitted by a power law with fixed spectral index (dotted line) and a modified blackbody with fixed emissivity (dashed line). The Draine & Lazarian (1998b) CNM spinning dust spectrum (dot-dashed line) has been fitted to the 31/33 GHz data.

generic and allow considerable freedom in the dust parameters (Finkbeiner 2004). A similar situation is observed in the H II region G159.6-18.5 (Watson et al. 2005) and the dark cloud LDN1622 (Casassus et al. 2006).

The Draine & Lazarian (1998b) models are expressed in terms of the intensity per hydrogen column density, in units of Jy sr^{-1} cm^2 per H atom. We estimate an average column density of hydrogen for RCW175 $N(\mathrm{H}) \approx 4.4 \times 10^{22}$ cm^{-22} using the canonical factor 2.13×10^{24} H cm^{-2} per unit of $\tau_{100\mu m}$ (Finkbeiner et al. 2004). The best-fitting spinning dust model in Figure 3 corresponds to $N(\mathrm{H}) = 4.4 \times 10^{22}$ cm^{-22}. The observed levels are therefore consistent with the emissivities of Draine & Lazarian (1998b). It is also remarkable that the amplitude of the anomalous component is similar to the emissivity relative to 100 μm observed at high Galactic latitudes (Davies et al. 2006), which is equivalent to 1 Jy at 30 GHz per 6000 Jy at 100 μm. This does not appear to be the case for all H II regions, which have so far been shown to have a reduced radio-to-dust emissivity (Dickinson et al. 2007; Scaife et al. 2007). High-resolution, multifrequency data in the range 10–100 GHz are needed to confirm this result and to investigate the nature of anomalous emission.

5. CONCLUSIONS

Using data from the VSA and CBI, we have observed excess emission at $\sim$ 30 GHz from the H II region RCW175. The flux density spectrum indicates that about half of the flux in this region is from optically thin free–free emission leaving about half unaccounted for. An upper limit at 94 GHz from *WMAP* data constrains the contribution of thermal dust emission. We have discarded optically thick free–free emission from UC H II regions and GPS sources as possible candidates for this excess; an upper limit at 94 GHz and high-resolution radio data rule these out as the primary contributor at $\sim$ 30 GHz. We interpret the excess as electric dipole radiation from small rapidly spinning dust grains as predicted by Draine & Lazarian (1998b). These models provide a reasonable fit to the data that is consistent both in terms of spectral shape and emissivity. High-resolution, multifrequency data in the range 10–100 GHz are needed to confirm this result and to investigate the nature of anomalous emission.

We thank the anonymous referee for useful comments. This work was supported by the Strategic Alliance for the Implementation of New Technologies (SAINT; see www.astro.caltech.edu/chajnantor/saint/index.html), and we are most grateful to the SAINT partners for their strong support. We gratefully acknowledge support from the Kavli Operating Institute and thank B. Rawn and S. Rawn, Jr. The CBI was supported by NSF grants 9802989, 0098734, and 0206416, and a Royal Society Small Research Grant. We are particularly indebted to the engineers who maintain and operate the CBI: C. Achermann, R. Bustos, C. Jara, N. Oyarace, R. Reeves, M. Shepherd, and C. Verdugo. C.D. thanks Roberta Paladini and Bill Reach for useful discussions. C.D. acknowledges support from the U.S. *Planck* project, which is funded by the NASA Science Mission Directorate. S.C. acknowledges support from FONDECYT grant 1030805, and from the Chilean Center for Astrophysics FONDAP 15010003. A.T. acknowledges support from Royal Society and STFC research fellowships.

REFERENCES

Altenhoff, W. J., Downes, D., Goad, L., Maxwell, A., & Rinehart, R. 1970, A&AS, 1, 319
Banday, A. J., Dickinson, C., Davies, R. D., Davis, R. J., & Górski, K. M. 2003, MNRAS, 345, 897
Beichman, C. A., Neugebauer, G., Habing, H. J., Clegg, P. E., & Chester, T. J. eds. 1988, in Infrared Astronomical Satellite (*IRAS*) Catalogs and Atlases, Explanatory Supplement, Vol. 1, NASA RP–1190 (Washington, DC: NASA)
Bennett, C. L., et al. 2003, ApJS, 148, 97
Bonaldi, A., Ricciardi, S., Leach, S., Stivoli, F., Baccigalupi, C., & de Zotti, G. 2007, MNRAS, 382, 1791
Casassus, S., Cabrera, G. F., Förster, F., Pearson, T. J., Readhead, A. C. S., & Dickinson, C. 2006, ApJ, 639, 951
Casassus, S., Nyman, L.-Å., Dickinson, C., & Pearson, T. J. 2007, MNRAS, 382, 1607
Casassus, S., Readhead, A. C. S., Pearson, T. J., Nyman, L.-Å., Shepherd, M. C., & Bronfman, L. 2004, ApJ, 603, 599
Condon, J. J., Cotton, W. D., Greisen, E. W., Yin, Q. F., Perley, R. A., Taylor, G. B., & Broderick, J. J. 1998, AJ, 115, 1693
Davies, R. D., Dickinson, C., Banday, A. J., Jaffe, T. R., Górski, K. M., & Davis, R. J. 2006, MNRAS, 370, 1125
de Oliveira-Costa, A., Tegmark, M., Davies, R. D., Gutiérrez, C. M., Lasenby, A. N., Rebolo, R., & Watson, R. A. 2004, ApJ, 606, L89
Dickinson, C., Casassus, S., Pineda, J. L., Pearson, T. J., Readhead, A. C. S., & Davies, R. D. 2006, ApJ, 643, L111
Dickinson, C., Davies, R. D., Bronfman, L., Casassus, S., Davis, R. J., Pearson, T. J., Readhead, A. C. S., & Wilkinson, P. N. 2007, MNRAS, 379, 297
Dickinson, C., Davies, R. D., & Davis, R. J. 2003, MNRAS, 341, 369

Dickinson, C., et al. 2004, MNRAS, 353, 732
Draine, B. T., & Lazarian, A. 1998a, ApJ, 494, L19+
Draine, B. T., & Lazarian, A. 1998b, ApJ, 508, 157
Draine, B. T., & Lazarian, A. 1999, ApJ, 512, 740
Dupac, X., et al. 2003, A&A, 404, L11
Fernández-Cerezo, S., et al. 2006, MNRAS, 370, 15
Finkbeiner, D. P. 2004, ApJ, 614, 186
Finkbeiner, D. P., Langston, G. I., & Minter, A. H. 2004, ApJ, 617, 350
Forbes, D. 1989, A&AS, 77, 439
Gordon, M. A. 1988, ApJ, 331, 509
Handa, T., Sofue, Y., Nakai, N., Hirabayashi, H., & Inoue, M. 1987, PASJ, 39, 709
Haynes, R. F., Caswell, J. L., & Simons, L. W. J. 1978, Aust. J. Phys. Astrophys. Suppl., 45, 1
Hildebrandt, S. R., Rebolo, R., Rubiño-Martín, J. A., Watson, R. A., Gutiérrez, C. M., Hoyland, R. J., & Battistelli, E. S. 2007, MNRAS, 382, 594
Hill, R. S., et al. 2008, ApJ, to be published (arXiv:0803.0570)
Hinshaw, G., et al. 2008, ApJ, to be published (arXiv:0803.0732)
Langston, G., Minter, A., D'Addario, L., Eberhardt, K., Koski, K., & Zuber, J. 2000, AJ, 119, 2801
Leitch, E. M., Readhead, A. C. S., Pearson, T. J., & Myers, S. T. 1997, ApJ, 486, L23
Padin, S., et al. 2002, PASP, 114, 83
Readhead, A. C. S., et al. 2004, ApJ, 609, 498
Reich, W., Fuerst, E., Reich, P., & Reif, K. 1990, A&AS, 85, 633
Rodgers, A. W., Campbell, C. T., & Whiteoak, J. B. 1960, MNRAS, 121, 103
Rybicki, G. B., & Lightman, A. P. 1979, in Radiative Processes in Astrophysics, (New York: Wiley Interscience) 393
Scaife, A., et al. 2007, MNRAS, 377, L69
Scaife, A. M. M., et al. 2008, MNRAS, 385, 809
Sharpless, S. 1959, ApJS, 4, 257
Watson, R. A., Rebolo, R., Rubiño-Martín, J. A., Hildebrandt, S., Gutiérrez, C. M., Fernández-Cerezo, S., Hoyland, R. J., & Battistelli, E. S. 2005, ApJ, 624, L89
Watson, R. A., et al. 2003, MNRAS, 341, 1057
Wood, D. O. S., & Churchwell, E. 1989, ApJS, 69, 831